# Atomic force calculations within the all-electron FLAPW method: Treatment of core states and discontinuities at the muffin-tin sphere boundary

Daniel A. Klüppelberg,* Markus Betzinger, and Stefan Blügel
*Peter Grünberg Institut and Institute for Advanced Simulation, Forschungszentrum Jülich and JARA, 52428 Jülich, Germany*
(Received 28 October 2014; published 5 January 2015)

We analyze the accuracy of the atomic force within the all-electron full-potential linearized augmented plane-wave (FLAPW) method using the force formalism of Yu *et al.* [Phys. Rev. B **43**, 6411 (1991)]. A refinement of this formalism is presented that explicitly takes into account the tail of high-lying core states leaking out of the muffin-tin sphere and considers the small discontinuities of LAPW wave function, density, and potential at the muffin-tin sphere boundaries. For MgO and $EuTiO_3$ it is demonstrated that these amendments substantially improve the acoustic sum rule and the symmetry of the force constant matrix. Sum rule and symmetry are realized with an accuracy of $\mu\mathrm{Htr}/a_\mathrm{B}$.

DOI: 10.1103/PhysRevB.91.035105 PACS number(s): 63.20.dk, 71.15.Mb

## I. INTRODUCTION

Nowadays, geometric, electronic, and magnetic properties for a wide range of real materials can be calculated routinely by density functional theory (DFT) [1,2] in the Kohn-Sham (KS) formalism [3]. Therein, the interacting many-electron system is mapped onto an auxiliary system of noninteracting electrons, whose ground-state density equals the ground-state density of the fully interacting system by construction. Physical quantities such as the ground-state total energy, magnetic moments, etc., can then be calculated as functions of the density.

These observables—in particular, the total energy—depend on the geometric structure of the system and the optimal geometry refers to the minimum of the total energy. For finding the optimal atomic positions in a given unit cell, atomic forces, i.e., the derivatives of the total energy with respect to the atomic positions, are an indispensable tool. In a given unit cell all forces on the atoms vanish at the energetically lowest structure. Exploiting the information about the energy landscape provided by the atomic forces, the optimal structure can be found by employing a numerical optimization procedure [4], whose speed of convergence improves typically with the quality of the forces.

Beyond that, atomic forces are utilized to calculate the frequency dispersion of lattice vibrations, so-called phonons, by means of the finite displacement method [5–7]. In this approach, one sets up a supercell, displaces one atom in the supercell in a certain direction, calculates the force on all other atoms, and repeats this procedure for a number of different atoms and directions [8]. The force constant matrix, which is the Hessian of the total energy, is then approximated by calculating the second derivative of the total energy through the difference quotient of the atomic forces. Due to the numerical differentiation of the atomic force, phonon calculations based on the finite displacement approach require a high accuracy of the calculated atomic force—in fact, typically a much higher accuracy than for structural optimization is required.

Atomic forces can be calculated within the full-potential linearized augmented plane-wave (FLAPW) method [9–11]—the benchmark choice among the electronic structure methods for solids—since the seminal work by Yu *et al.* [12] and Soler and Williams [13,14]. Both groups demonstrated that the explicit dependence of the LAPW basis functions on the atomic positions leads to an additional and important contribution to the atomic force, the so-called Pulay term [15], and gave expressions to evaluate this term. While the Pulay term would not be present in a purely plane-wave-based approach, the Pulay term is essential for calculating reliable forces within the LAPW methodology. In contrast to Yu *et al.*, Soler and Williams have chosen a particular formulation of the LAPW method, in which the basis functions are strictly continuous at the muffin-tin (MT) sphere boundary, which separates the volume inside the atomic sphere from the interstitial region (IR) between the spheres. In the limit of infinite numerical cutoff parameters, the formulations of both groups should become identical [16,17].

In this work, we revisit the force formulation within the FLAPW method in the light of the high accuracy demands required for phonon calculations based on the finite displacement approach. The starting point of our considerations is the force formalism of Yu *et al.* [12]. According to the acoustic sum rule the sum of all atomic forces within the unit cell has to vanish. While this is a strict, theoretical prescription resulting from the translational invariance of the system, we found deviations from this rule up to $10^{-4}\mathrm{Htr}/a_\mathrm{B}$ in practice. The fulfillment of this sum rule is vital to guarantee that the three acoustic phonon branches at the zone center of the Brillouin zone have zero energy. We demonstrate, moreover, that the force calculated according to Yu *et al.* [12] might lead to a force constant matrix that substantially deviates from a symmetric form.

We have been able to trace back these issues to mainly two sources: (a) energetically high-lying core states whose wave functions exhibit a substantial tail out of the muffin-tin into the interstitial region; (b) an improper treatment of the small discontinuities of the LAPW wave functions, density, and potential at the MT sphere boundary for finite numerical cutoff parameters. We propose a refined force formalism that explicitly takes into account both the tail of high-lying core states as well as the discontinuities at the muffin-tin sphere boundary. We show for rocksalt MgO and perovskite $EuTiO_3$ that these amendments improve the fulfillment of the acoustic sum rule and the symmetry of the force-constant matrix by up to three orders of magnitude.

*d.a.klueppelberg@fz-juelich.de

 

The paper is organized as follows. In Sec. II we give a brief introduction into the KS formalism and the FLAPW approach. All quantities, which are required later on, are introduced and defined. We derive a refined force formula in Sec. III taking into account the tail of the core states as well as the discontinuities at the MT sphere boundaries. The improvements of the new force formula are demonstrated in Sec. IV. Finally, we draw our conclusions in Sec. V.

## II. KOHN-SHAM DFT AND THE FLAPW APPROACH

The KS [3] formalism of DFT is based on an auxiliary system of noninteracting electrons, the so-called KS system. These noninteracting electrons move in an effective potential $V_{\text{eff}}(\mathbf{r})$, which consists of the external potential $V_{\text{ext}}(\mathbf{r})$ generated by the charges of the atomic nuclei, the classical electrostatic Hartree potential $V_{\text{H}}(\mathbf{r})$, and an exchange-correlation (xc) potential $V_{\text{xc}}(\mathbf{r})$. The ground-state density of the KS system coincides by construction with that of the true interacting system. By solving the noninteracting KS equations

$$[H_{\text{KS}} - \epsilon_{n\mathbf{k}}]\varphi_{n\mathbf{k}}(\mathbf{r}) = 0, \tag{1}$$

the electron density is given by

$$n(\mathbf{r}) = \sum_{n\mathbf{k}} f_{n\mathbf{k}} |\varphi_{n\mathbf{k}}(\mathbf{r})|^2, \tag{2}$$

where $\varphi_{n\mathbf{k}}(\mathbf{r})$ are the KS orbitals, $n$ is the band index, $\mathbf{k}$ denotes the Bloch vector, $\epsilon_{n\mathbf{k}}$ is the KS one-particle energy of orbital $\varphi_{n\mathbf{k}}$, $H_{\text{KS}} = -\frac{1}{2}\nabla^2 + V_{\text{eff}}(\mathbf{r})$ defines the KS Hamiltonian, and $f_{n\mathbf{k}}$ is the occupation number of orbital $\varphi_{n\mathbf{k}}$. We employ Hartree atomic units throughout this paper and the spin index is suppressed for simplicity.

The ground-state energy $E$ of the interacting system can then be calculated from

$$E[n] = T_0[n] + E_{\text{H}}[n] + E_{\text{ext}}[n] + E_N + E_{\text{xc}}[n], \tag{3}$$

where $T_0[n] = \sum_{n\mathbf{k}} f_{n\mathbf{k}}\epsilon_{n\mathbf{k}} - \int n(\mathbf{r})V_{\text{eff}}(\mathbf{r})d^3r$ is the kinetic energy of the KS electrons, $E_{\text{H}}[n] = \frac{1}{2}\iint \frac{n(\mathbf{r})n(\mathbf{r}')}{|\mathbf{r}-\mathbf{r}'|}d^3r d^3r'$ denotes the Hartree energy, $E_{\text{ext}}[n] = \int n(\mathbf{r})V_{\text{ext}}(\mathbf{r})d^3r$ corresponds to the energy contribution caused by the external potential, and $E_N$ is the electrostatic repulsion energy between the point charges of the atomic nuclei. All exchange and correlation energy contributions of the interacting many-electron system are hidden in the xc energy $E_{\text{xc}}[n]$. The exact form of the latter is, in general, unknown. Hence, it must be approximated and we will make use of the local density approximation [18,19], which has the generic form

$$E_{\text{xc}}[n] = \int n(\mathbf{r})\epsilon_{\text{xc}}[n(\mathbf{r})]d^3r. \tag{4}$$

The all-electron FLAPW method [9–11] is one specific approach to solve the KS equations. The core states, which are strongly bound to the atomic nuclei, are described by solving the Dirac equation for the spherical part of the effective KS potential. The valence electron states and their wave functions, on the other hand, are represented through the LAPW basis set $\{\chi_{\mathbf{kG}}(\mathbf{r})\}$,

$$\varphi_{n\mathbf{k}}(\mathbf{r}) = \sum_{\mathbf{G}} z_{\mathbf{G}}(n\mathbf{k})\chi_{\mathbf{kG}}(\mathbf{r}), \tag{5}$$

where $z_{\mathbf{G}}(n\mathbf{k})$ are the expansion coefficients of the wave function. The basis is defined piecewise in order to cope at the same time with the rapid oscillations of the wave functions close to the atomic nuclei and their rather smooth form in the region far away from the nuclei. Accordingly, space is partitioned into so-called muffin-tin spheres around each atomic nucleus and a remaining interstitial region between these spheres. In each MT sphere the LAPW basis consists of numerical radial functions and spherical harmonics. Per angular momentum $l$ one uses two radial functions: the solution to the spherical KS equation $u_l(r)$ and its energy derivative $\dot{u}_l(r)$. In the remaining IR, where the wave function is smooth, plane waves are employed as basis functions. IR and MT representations are matched at each sphere boundary in value and slope. Thus, the LAPW basis function of Bloch vector $\mathbf{k}$ and reciprocal lattice vector $\mathbf{G}$ is given by

$$\chi_{\mathbf{kG}}(\mathbf{r}) = \begin{cases} \frac{1}{\sqrt{\Omega}}\exp[i(\mathbf{k}+\mathbf{G})\cdot\mathbf{r}], & \mathbf{r} \in \text{IR} \\ \sum_{lm}\left[a^{\alpha}_{lm}(\mathbf{kG})u^{\alpha}_{l}(|\mathbf{r}-\boldsymbol{\tau}_\alpha|) + b^{\alpha}_{lm}(\mathbf{kG})\dot{u}^{\alpha}_{l}(|\mathbf{r}-\boldsymbol{\tau}_\alpha|)\right]Y_{lm}(\mathbf{r}-\boldsymbol{\tau}_\alpha), & \mathbf{r} \in \text{MT}(\alpha) \end{cases} \tag{6}$$

with the unit cell volume $\Omega$ and the matching coefficients $a^{\alpha}_{lm}(\mathbf{kG})$, $b^{\alpha}_{lm}(\mathbf{kG})$ in the MT sphere of atom $\alpha$ placed at position $\boldsymbol{\tau}_\alpha$. The size of the LAPW basis is controlled by the reciprocal cutoff value $G_{\max}$, i.e., all reciprocal lattice vectors $\mathbf{G}$ with $|\mathbf{k}+\mathbf{G}| \leqslant G_{\max}$ form the set of basis functions at Bloch vector $\mathbf{k}$. Furthermore, the angular momentum expansion in the MT spheres is truncated at $l_{\max}$.

The choice of the muffin-tin radii derives from the argument that the atomic spheres should be maximally space filling, but to allow for structural relaxation, the radii are required to be chosen such that different atomic spheres are not colliding. Also, the spheres should be large enough to host all core electrons while being not too large that the basis set leads to significant linearization errors [20]. This compromise is sometimes difficult to achieve.

In order to increase the flexibility of the basis within the MT spheres, so-called local orbitals [20–24] can be added to the set of augmented plane-waves. These additional basis functions are only nonzero within the MT sphere and have zero value and slope at the MT sphere boundary.

We note that the wave functions of energetically high-lying core states may extend beyond the MT sphere of the corresponding atom: They might exhibit a tail in the IR and might even reach the MT spheres of adjacent atoms (see, for an example, Fig. 1). The most rigorous, but numerically also most expensive way of treating such semicore states is to describe

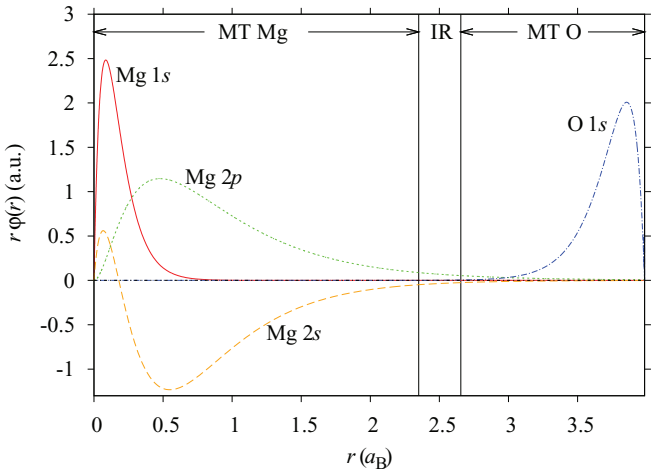


FIG. 1. (Color online) Core states of MgO along the [100] direction. The Mg atom is located at the origin ($r = 0$), where the O atom is placed at $r = 3.985a_B$. The MT spheres of the Mg and O atoms as well as the interstitial region are marked.

them as valence-electron states by adding local orbitals. Then, the tail of the core state is described by the LAPW basis set. To our experience, for many systems the addition of local orbitals is not absolutely necessary provided that the charge of the leaking core tail does not contribute to resonant bonding and is properly added to the MT and IR density. Therefore, the core electron wave functions are computed on a sufficiently large radial grid that goes beyond the MT radius. Subsequently, the core charge inside the spheres is replaced by a Gaussian-like pseudodensity that matches the tail outside the sphere in value and slope at the sphere boundary. The pseudocharge density is then Fourier transformed and added to the IR and MT charge density. For the latter, the Fourier transform is reexpanded in spherical harmonics centered at the MT sphere of all other atoms in the unit cell.

Likewise to the wave functions, the all-electron potential and density are expanded into symmetry-adapted plane-waves in the IR and numerical radial functions times symmetry-adapted spherical harmonics in the MT spheres [25].

We finally note that due to the finite angular momentum cutoff $l_{\max}$ the KS valence electron wave functions and thus the density and potential are continuous in value and slope only up to $l_{\max}$.

## III. ATOMIC FORCES OF KS DFT

We derive in the following a revised atomic force formula within the LAPW approach, where special attention is paid to both the atomic-position dependence of the LAPW basis and the partitioning of space into atomic-position-dependent regions. In conjunction with the (small) discontinuities of LAPW basis functions, density, and potential at the MT sphere boundaries, this partitioning gives rise to a series of MT surface terms, of which only the one involving the kinetic energy has been taken into account in the work of Yu *et al.* [12].

We keep the derivation of the force formula quite general, as we believe that these considerations might be important for other all-electron methods that rely on a partitioning of space into atomic-position-dependent regions and use an atomic-position-dependent basis—as, for example, the linear muffin-tin orbital approach [26–28]. Details of the implementation are given in Sec. III A. In particular, in contrast to Yu *et al.* [12] we do not assume that the core electrons are strictly confined to the MT spheres. Furthermore, we use the proper IR representation for the basis, density, and potential in the MT surface terms.

The force exerted on atom $\alpha$ residing at position $\boldsymbol{\tau}_\alpha$ is defined as

$$\mathbf{F}_\alpha = -\frac{dE[n]}{d\boldsymbol{\tau}_\alpha} \tag{7}$$

and thus points in the direction of the greatest decrease of the total energy.

In order to calculate the force each term in Eq. (3) has to be differentiated with respect to $\boldsymbol{\tau}_\alpha$. Most of the energy contributions to the total energy involve an integral over space. Due to the partitioning of space into atom-centered MT spheres and the interstitial region the derivative of these spatial integrals consists of two parts: one that arises from the derivative of the integrand and the second one from the derivative of the integration domain with respect to the atomic position $\boldsymbol{\tau}_\alpha$. The latter gives rise to a surface term on the MT sphere boundary of atom $\alpha$. The derivative of the generic integral $\int f(\mathbf{r})d^3r$ with respect to $\boldsymbol{\tau}_\alpha$ thus yields

$$\begin{aligned}
&\frac{d}{d\boldsymbol{\tau}_\alpha}\int f(\mathbf{r})\,d^3r \\
&= \frac{d}{d\boldsymbol{\tau}_\alpha}\left[\sum_\beta \int_{\mathrm{MT}(\beta)} f(\mathbf{r})\,d^3r + \int_{\mathrm{IR}} f(\mathbf{r})\,d^3r\right] \\
&= \sum_\beta \int_{\mathrm{MT}(\beta)} \frac{df(\mathbf{r})}{d\boldsymbol{\tau}_\alpha}\,d^3r + \int_{\mathrm{IR}} \frac{df(\mathbf{r})}{d\boldsymbol{\tau}_\alpha}\,d^3r \\
&\quad + \oint_{\partial\mathrm{MT}(\alpha)} [f^{\mathrm{MT}}(\mathbf{r}) - f^{\mathrm{IR}}(\mathbf{r})]\hat{\mathbf{e}}\,dS,
\end{aligned} \tag{8}$$

where the surface integral runs over the MT sphere boundary $\partial$MT of atom $\alpha$, $\hat{\mathbf{e}} = \frac{\mathbf{r}-\boldsymbol{\tau}_\alpha}{|\mathbf{r}-\boldsymbol{\tau}_\alpha|}$ denotes the normal vector on the MT sphere of atom $\alpha$ that points into the IR, and $f^{\mathrm{MT}}(\mathbf{r})$ and $f^{\mathrm{IR}}(\mathbf{r})$ distinguish between the MT and IR representations of the quantity $f$. For continuous integrands $f(\mathbf{r})$, the surface contribution vanishes. But due to the inevitable usage of finite cutoff values in the representation of the basis functions, the density, and the potential, those quantities typically exhibit a small discontinuity at the sphere boundary in all practical calculations, so that the surface term $\oint_{\partial\mathrm{MT}(\alpha)}[f^{\mathrm{MT}}(\mathbf{r}) - f^{\mathrm{IR}}(\mathbf{r})]\hat{\mathbf{e}}\,dS$ does persist.

Bearing this in mind the force on atom $\alpha$ is given by

$$\begin{aligned}
\mathbf{F}_\alpha = \mathbf{F}_\alpha^{\mathrm{HF}} &- \sum_{n\mathbf{k}} f_{n\mathbf{k}} \frac{d\epsilon_{n\mathbf{k}}}{d\boldsymbol{\tau}_\alpha} + \int n(\mathbf{r})\frac{dV_{\mathrm{eff}}(\mathbf{r})}{d\boldsymbol{\tau}_\alpha}d^3r \\
&- \oint_{\partial\mathrm{MT}(\alpha)} n^{\mathrm{MT}}(\mathbf{r})\left[\epsilon_{\mathrm{xc}}^{\mathrm{MT}}(\mathbf{r}) - V_{\mathrm{xc}}^{\mathrm{MT}}(\mathbf{r})\right]\hat{\mathbf{e}}\,dS \\
&+ \oint_{\partial\mathrm{MT}(\alpha)} n^{\mathrm{IR}}(\mathbf{r})\left[\epsilon_{\mathrm{xc}}^{\mathrm{IR}}(\mathbf{r}) - V_{\mathrm{xc}}^{\mathrm{IR}}(\mathbf{r})\right]\hat{\mathbf{e}}\,dS\,,
\end{aligned} \tag{9}$$

where we introduced the Hellmann-Feynman force

$$\mathbf{F}_\alpha^{\mathrm{HF}} = -\int n(\mathbf{r})\frac{dV_{\mathrm{ext}}(\mathbf{r})}{d\boldsymbol{\tau}_\alpha}\,d^3r - \frac{dE_N}{d\boldsymbol{\tau}_\alpha}. \tag{10}$$

For a metal, where the steplike distinction between occupied and unoccupied states is artificially smeared out to improve the convergence of the self-consistent-field cycle, also the variation of the occupation number $f_{n\mathbf{k}}$ has to be taken into account in Eq. (9). It has been shown in Ref. [29], however, that the term resulting from the variation of $f_{n\mathbf{k}}$ exactly cancels with an entropylike term that has to be added to the total energy in this case to retain the variational property of the energy with respect to the density.

The derivative of the KS eigenvalue $\epsilon_{n\mathbf{k}}$ with respect to $\boldsymbol{\tau}_\alpha$ can be evaluated by making use of the Rayleigh coefficient and relation (8):

$$\begin{aligned}\frac{d\epsilon_{n\mathbf{k}}}{d\boldsymbol{\tau}_\alpha} &= \frac{d}{d\boldsymbol{\tau}_\alpha}\frac{\int \varphi^*_{n\mathbf{k}}(\mathbf{r})H_{\mathrm{KS}}\varphi_{n\mathbf{k}}(\mathbf{r})d^3r}{\int \varphi^*_{n\mathbf{k}}(\mathbf{r})\varphi_{n\mathbf{k}}(\mathbf{r})d^3r}\\ &= \langle d\varphi_{n\mathbf{k}}/d\boldsymbol{\tau}_\alpha|H_{\mathrm{KS}}-\epsilon_{n\mathbf{k}}|\varphi_{n\mathbf{k}}\rangle + \mathrm{c.c.}\\ &\quad + \oint_{\partial\mathrm{MT}(\alpha)} \varphi^{\mathrm{MT}*}_{n\mathbf{k}}(\mathbf{r})[H_{\mathrm{KS}}-\epsilon_{n\mathbf{k}}]\varphi^{\mathrm{MT}}_{n\mathbf{k}}(\mathbf{r})\hat{\mathbf{e}}\,dS\\ &\quad - \oint_{\partial\mathrm{MT}(\alpha)} \varphi^{\mathrm{IR}*}_{n\mathbf{k}}(\mathbf{r})[H_{\mathrm{KS}}-\epsilon_{n\mathbf{k}}]\varphi^{\mathrm{IR}}_{n\mathbf{k}}(\mathbf{r})\hat{\mathbf{e}}\,dS\\ &\quad + \int |\varphi_{n\mathbf{k}}(\mathbf{r})|^2\frac{dV_{\mathrm{eff}}(\mathbf{r})}{d\boldsymbol{\tau}_\alpha}d^3r. \end{aligned} \tag{11}$$

Combining Eqs. (9) and (11) then yields

$$\mathbf{F}_\alpha = \mathbf{F}^{\mathrm{HF}}_\alpha - \mathbf{F}^{\mathrm{Pulay}}_\alpha - \mathbf{F}^{\mathrm{surface}}_\alpha \tag{12}$$

with the Pulay force

$$\mathbf{F}^{\mathrm{Pulay}}_\alpha = \sum_{n\mathbf{k}} f_{n\mathbf{k}}\langle d\varphi_{n\mathbf{k}}/d\boldsymbol{\tau}_\alpha|H_{\mathrm{KS}}-\epsilon_{n\mathbf{k}}|\varphi_{n\mathbf{k}}\rangle + \mathrm{c.c.} \tag{13}$$

and a surface force contribution

$$\begin{aligned}\mathbf{F}^{\mathrm{surface}}_\alpha &= \oint_{\partial\mathrm{MT}(\alpha)} \Big\{n^{\mathrm{MT}}(\mathbf{r})\big[\epsilon^{\mathrm{MT}}_{\mathrm{xc}}(\mathbf{r}) + V^{\mathrm{MT}}_{\mathrm{eff}}(\mathbf{r}) - V^{\mathrm{MT}}_{\mathrm{xc}}(\mathbf{r})\big]\\ &\quad - n^{\mathrm{IR}}(\mathbf{r})\big[\epsilon^{\mathrm{IR}}_{\mathrm{xc}}(\mathbf{r}) + V^{\mathrm{IR}}_{\mathrm{eff}}(\mathbf{r}) - V^{\mathrm{IR}}_{\mathrm{xc}}(\mathbf{r})\big]\Big\}\hat{\mathbf{e}}\,dS\\ &\quad + \sum_{n\mathbf{k}} f_{n\mathbf{k}}\oint_{\partial\mathrm{MT}(\alpha)} \Big\{\varphi^{\mathrm{MT}*}_{n\mathbf{k}}(\mathbf{r})[T-\epsilon_{n\mathbf{k}}]\varphi^{\mathrm{MT}}_{n\mathbf{k}}(\mathbf{r})\\ &\quad - \varphi^{\mathrm{IR}*}_{n\mathbf{k}}(\mathbf{r})[T-\epsilon_{n\mathbf{k}}]\varphi^{\mathrm{IR}}_{n\mathbf{k}}(\mathbf{r})\Big\}\hat{\mathbf{e}}\,dS. \end{aligned} \tag{14}$$

The Pulay term $\mathbf{F}^{\mathrm{Pulay}}_\alpha$ would exactly vanish, if either the basis used for expanding the KS wave functions does not depend on the atomic positions—this is the trivial case—or if the KS wave functions $\varphi_{n\mathbf{k}}$ were exact pointwise solutions to the KS Hamiltonian. Neither the first nor the second condition is fulfilled in the LAPW approach. In fact, in the LAPW method the Pulay term represents an important contribution to the force, which cannot be neglected. This is one of central results of the paper of Yu *et al.* [12].

The force formula (12) differs from the one derived in the aforementioned paper in the surface force term. Yu *et al.* restricted their considerations to the discontinuity in the second derivative of the wave functions giving rise to a surface term of the form

$$\sum_{n\mathbf{k}} f_{n\mathbf{k}}\oint_{\partial\mathrm{MT}(\alpha)} \big\{\varphi^{\mathrm{MT}*}_{n\mathbf{k}}(\mathbf{r})T\varphi^{\mathrm{MT}}_{n\mathbf{k}}(\mathbf{r}) - \varphi^{\mathrm{IR}*}_{n\mathbf{k}}(\mathbf{r})T\varphi^{\mathrm{IR}}_{n\mathbf{k}}(\mathbf{r})\big\}\hat{\mathbf{e}}\,dS, \tag{15}$$

which corresponds to Eq. 20(b) of their paper. This term is naturally included in Eq. (14). But in addition, Eq. (14) encompasses contributions arising from the discontinuity of the density and potential at the sphere boundary. Hence, the surface term $\mathbf{F}^{\mathrm{surface}}_\alpha$, Eq. (14), is more general than the one considered in Ref. [12].

We proceed by discussing the evaluation of the Pulay and surface term in the FLAPW approach [30].

### A. Pulay force term

The Pulay term, Eq. (13), involves a sum over all occupied states comprising core and valence electron states. While the core electron wave functions are found by solving an atomic scalar-relativistic or fully-relativistic Dirac equation for the spherical effective KS potential, the valence electrons are represented through the LAPW basis (6). Hence, we discuss the evaluation of the Pulay term separately for core and valence electron states. We first focus on the latter. According to (5) the variation of the valence states with respect to $\boldsymbol{\tau}_\alpha$ consists of two contributions

$$\frac{d\varphi_{n\mathbf{k}}(\mathbf{r})}{d\boldsymbol{\tau}_\alpha} = \sum_{\mathbf{G}}\frac{dz_{\mathbf{G}}(n\mathbf{k})}{d\boldsymbol{\tau}_\alpha}\chi_{\mathbf{kG}}(\mathbf{r}) + z_{\mathbf{G}}(n\mathbf{k})\frac{d\chi_{\mathbf{kG}}(\mathbf{r})}{d\boldsymbol{\tau}_\alpha}. \tag{16}$$

For the Pulay force term only the second term is vital, as the first one stays within the Hilbert space spanned by the LAPW basis functions $\chi_{\mathbf{kG}}(\mathbf{r})$, in which the Schrödinger equation is fulfilled variationally. Thus, the first term yields exactly zero when plugged into Eq. (13).

The LAPW basis functions exhibit a dependence on the atomic positions only in the MT spheres and there through the matching coefficients $a^\alpha_{lm}(\mathbf{kG})$, $b^\alpha_{lm}(\mathbf{kG})$ as well as through the radial functions and spherical harmonics, which are defined with respect to the atomic position $\boldsymbol{\tau}_\alpha$ and depend on the effective potential. If we disregard changes of the LAPW basis that are caused by variations in the effective potential, the derivative of the LAPW basis function with respect to the atomic position $\boldsymbol{\tau}_\alpha$ is given by

$$\frac{d\chi_{\mathbf{kG}}(\mathbf{r})}{d\boldsymbol{\tau}_\alpha} = \begin{cases} i(\mathbf{k}+\mathbf{G})\chi_{\mathbf{kG}}(\mathbf{r}) - \nabla\chi_{\mathbf{kG}}(\mathbf{r}), & \mathbf{r}\in\mathrm{MT}(\alpha)\\ 0, & \text{else,}\end{cases} \tag{17}$$

where the first term results from the derivative of the matching coefficients and the second from the explicit derivative of radial function times spherical harmonic. Inserting Eq. (17) in Eq. (13) and performing similar steps as explained in the Appendix of Ref. [12] we obtain the Pulay force term for the valence (val) electrons

$$\begin{aligned}\mathbf{F}^{\mathrm{Pulay}}_{\alpha,\mathrm{val}} &= \sum_{n\mathbf{k}}^{\mathrm{val}} f_{n\mathbf{k}}\sum_{\mathbf{G},\mathbf{G}'} i(\mathbf{G}'-\mathbf{G})z^*_{\mathbf{G}}(n\mathbf{k})z_{\mathbf{G}'}(n\mathbf{k})\\ &\quad\times\langle\chi_{\mathbf{kG}}|H_{\mathrm{KS}}-\epsilon_{n\mathbf{k}}|\chi_{\mathbf{kG}'}\rangle|_{\mathrm{MT}(\alpha)}\\ &\quad - \sum_{n\mathbf{k}}^{\mathrm{val}} f_{n\mathbf{k}}\oint_{\partial\mathrm{MT}(\alpha)}\varphi^{\mathrm{MT}*}_{n\mathbf{k}}(\mathbf{r})[T-\epsilon_{n\mathbf{k}}]\varphi^{\mathrm{MT}}_{n\mathbf{k}}(\mathbf{r})\hat{\mathbf{e}}\,dS\\ &\quad - \int_{\mathrm{MT}(\alpha)} V_{\mathrm{eff}}(\mathbf{r})\nabla n_{\mathrm{val}}(\mathbf{r})d^3r, \end{aligned} \tag{18}$$

where $\langle\cdot|\cdot|\cdot\rangle|_{\mathrm{MT}(\alpha)}$ means that the integration domain is restricted to the MT sphere of atom $\alpha$ and $n_{\mathrm{val}}(\mathbf{r}) = \sum_{n\mathbf{k}}^{\mathrm{val}} f_{n\mathbf{k}}|\varphi_{n\mathbf{k}}(\mathbf{r})|^2$ denotes the valence electron charge. The surface integral $\oint_{\partial\mathrm{MT}(\alpha)} \varphi_{n\mathbf{k}}^{\mathrm{MT}*}(\mathbf{r})[T-\epsilon_{n\mathbf{k}}]\varphi_{n\mathbf{k}}^{\mathrm{MT}}(\mathbf{r})\hat{\mathbf{e}}dS$ results from the two volume integrals, $\langle\nabla\varphi_{n\mathbf{k}}|T-\epsilon_{n\mathbf{k}}|\varphi_{n\mathbf{k}}\rangle|_{\mathrm{MT}(\alpha)} + \langle\varphi_{n\mathbf{k}}|T-\epsilon_{n\mathbf{k}}|\nabla\varphi_{n\mathbf{k}}\rangle|_{\mathrm{MT}(\alpha)}$, by making use of Gauss' theorem.

Next, we address the contribution of the core electrons to the Pulay force term. Due to their atomiclike treatment the core electron wave functions $\varphi_{n\mathbf{k}}^{\mathrm{core}}(\mathbf{r})$ exhibit only a formal $\mathbf{k}$ dependence and the quantum number $n$ must be understood as a superindex $n = (\beta plm_l)$ comprising the atom $\beta$, the principal quantum number $p$, the angular momentum $l$, and the magnetic quantum number $m_l$. If one solves the fully-relativistic instead of the scalar-relativistic Dirac equation for the core states, the tuple $l,m_l$ has to be replaced by the total angular momentum $j$ and its projection $m_j$. Making the same assumption as for the valence electrons, i.e., neglecting the variation of the core electrons due to the change in the effective potential resulting from the infinitesimal change in the position of atom $\alpha$, the derivative of the core state $\varphi_{n\mathbf{k}}^{\mathrm{core}}(\mathbf{r})$ with respect to $\boldsymbol{\tau}_\alpha$ obeys

$$\frac{d\varphi_{n\mathbf{k}}^{\mathrm{core}}(\mathbf{r})}{d\boldsymbol{\tau}_\alpha} = -\nabla\varphi_{n\mathbf{k}}^{\mathrm{core}}(\mathbf{r})\delta_{\alpha\beta}, \tag{19}$$

where the Kronecker delta function $\delta_{\alpha\beta}$ means that only those core states are affected that are centered at the moving atom $\alpha$. With this relation the Pulay term for the core electrons becomes

$$\begin{aligned}\mathbf{F}_{\alpha,\mathrm{core}}^{\mathrm{Pulay}} &= -\sum_{n\mathbf{k}}^{\mathrm{core}} \delta_{\alpha\beta}\left[\left\langle\nabla\varphi_{n\mathbf{k}}^{\mathrm{core}}\middle|T-\epsilon_{n\mathbf{k}}\middle|\varphi_{n\mathbf{k}}^{\mathrm{core}}\right\rangle + \mathrm{c.c.}\right] \\ &\quad - \int V_{\mathrm{eff}}(\mathbf{r})\nabla n_{\mathrm{core}}^{\alpha}(\mathbf{r})d^3r \\ &= -\int V_{\mathrm{eff}}(\mathbf{r})\nabla n_{\mathrm{core}}^{\alpha}(\mathbf{r})d^3r \end{aligned} \tag{20}$$

and $n_{\mathrm{core}}^{\alpha}(\mathbf{r}) = \sum_{n\mathbf{k}}^{\mathrm{core}} \delta_{\alpha\beta}|\varphi_{n\mathbf{k}}^{\mathrm{core}}(\mathbf{r})|^2$. The first term involving the sum over the core electron states of atom $\alpha$ vanishes as it can be transformed into a surface integral over the unit-cell border with a lattice periodic integrand by means of Gauss' theorem. A surface term on the MT sphere boundary does not occur since the core states are per construction continuous to any order. Details concerning the implementation of Eq. (20) are given in Appendix A.

However, it is important to note that the remaining integral runs over the whole unit cell and its domain is not restricted to the MT sphere of atom $\alpha$, since the core density $n_{\mathrm{core}}^{\alpha}(\mathbf{r})$ is not necessarily confined to the MT sphere of atom $\alpha$. In fact, the tail of the core density of atom $\alpha$ can extend into the interstitial region and might even reach other MT spheres as demonstrated in Fig. 1 for the case of MgO. This is another point, where our formalism deviates from the one proposed by Yu *et al.* [12]. They assumed that the muffin-tin radius was chosen such that the core states and thus the core state density are already decayed to zero at the MT sphere boundary and thus restrict the integration domain in Eq. (20) to the MT sphere of atom $\alpha$. However, it turns out in practice that for many systems the muffin-tin radii cannot be chosen such that this requirement is fulfilled. Of course, by describing the energetically high-lying core states with local orbitals as valence states, the assumption of Yu *et al.* can always be enforced; however, at the price that the calculations become computationally more involved.

The complete Pulay force acting on atom $\alpha$ is then given by adding up its valence and core contribution:

$$\mathbf{F}_{\alpha}^{\mathrm{Pulay}} = \mathbf{F}_{\alpha,\mathrm{val}}^{\mathrm{Pulay}} + \mathbf{F}_{\alpha,\mathrm{core}}^{\mathrm{Pulay}}. \tag{21}$$

### B. Surface force term

Finally, we turn to the surface force term, Eq. (14). For the valence electrons, the integral containing the kinetic energy operator evaluated with the MT representation cancels with the corresponding contribution from the Pulay force in Eq. (18):

$$\begin{aligned}&\mathbf{F}_{\alpha,\mathrm{kin}}^{\mathrm{Pulay}} + \mathbf{F}_{\alpha,\mathrm{kin}}^{\mathrm{surface}} \\ &\quad = -\sum_{n\mathbf{k}}^{\mathrm{val}} f_{n\mathbf{k}} \oint_{\partial\mathrm{MT}(\alpha)} \varphi_{n\mathbf{k}}^{\mathrm{IR}*}(\mathbf{r})[T-\epsilon_{n\mathbf{k}}]\varphi_{n\mathbf{k}}^{\mathrm{IR}}(\mathbf{r})\hat{\mathbf{e}}\,dS. \end{aligned} \tag{22}$$

For the core electrons the terms related to the kinetic energy operator vanish, as the core states are continuous at the MT sphere boundary by construction. The remaining part of the surface force term is evaluated as it stands, i.e., we evaluate each surface integral by using the respective representation of the involved quantities. We emphasize that we do not replace in Eq. (22) the IR representation of the basis functions on the MT sphere boundary by the respective MT representation as it is done in the paper of Yu *et al.* [cf. Eq. (A9) ff. of Ref. [12]]. Details concerning the evaluation of the surface integrals involving the IR plane-wave representation are given in Appendix B.

## IV. PERFORMANCE OF THE REVISED FORCE FORMULA

In the following, we apply the previously developed force formalism to rocksalt MgO and the ferromagnetic perovskite $EuTiO_3$ and analyze its performance. Emphasis is laid on the improvements gained through the inclusion of the core tails and the consideration of the discontinuities at the MT sphere boundaries. In order to point out the amendments in comparison to the formalism of Yu *et al.* [12] and to show the impact of the different terms, we define a hierarchy of four levels, by which we address the different contributions:

LEVEL 0. The force is calculated as described by Yu *et al.* in Ref. [12].

LEVEL 1. The assumption that the core electrons are confined to their respective MT sphere is abandoned, which corresponds to integrating over the whole unit cell in Eq. (20).

LEVEL 2. The surface term involving the kinetic energy, Eq. (22), is calculated with the proper representation of the IR wave function at the boundary.

LEVEL 3. All additional surface terms of Eq. (14) are taken into account.

For each LEVEL only the differences in comparison to the previous one are explained.

We assess the four different LEVELS by comparing the force obtained from the analytic differentiation of the total energy with its numerically differentiated counterpart in Sec. IV A, by analyzing the spurious drift force in Sec. IV B,

TABLE I. Summary of the employed numerical parameters for MgO in rocksalt and ferromagnetic $EuTiO_3$ in perovskite structure. These parameters are used, if not stated otherwise.

| MgO | | | $EuTiO_3$ | | |
|---|---|---|---|---|---|
| $a_0$ | = | $7.970a_B$ | $a_0$ | = | $7.370a_B$ |
| $R_{Mg}$ | = | $2.35a_B$ | $R_{Eu}$ | = | $2.60a_B$ |
| $R_O$ | = | $1.33a_B$ | $R_{Ti}$ | = | $2.21a_B$ |
| | | | $R_O$ | = | $1.41a_B$ |
| $G_{max}$ | = | $5.50a_B^{-1}$ | $G_{max}$ | = | $4.80a_B^{-1}$ |
| $G_{max}^{dop}$ | = | $22.01a_B^{-1}$ | $G_{max}^{dop}$ | = | $28.81a_B^{-1}$ |
| $l_{max}$ | = | 14 | $l_{max}$ | = | 12 |
| $Mg_{core}$: | | $[He]2s2p$ | $Eu_{core}$: | | $[Kr]4d$ |
| $O_{core}$: | | $1s$ | $Ti_{core}$: | | $[Ne]3s$ |
| | | | $O_{core}$: | | $1s$ |
| LOs : | | – | LOs : | | $Eu_{5s,5p}Ti_{3p}$ |

by examining the symmetry of the force constant matrix in Sec. IV C, and finally by giving computational timings in Sec. IV D.

Before we start with the discussion we summarize the employed numerical parameters for the two systems MgO and $EuTiO_3$. For both systems a $10\times10\times10$ Monkhorst Pack grid is applied to sample the Brillouin zone (BZ). For all atoms in the unit cell the same angular momentum cutoff $l_{max}$ is used for the expansion of the wave functions, charge density, and potential inside the MT sphere. An expansion of the charge density up to $2l_{max}$ did not result in a measurable improvement of the forces and is not discussed further. The actual value of $l_{max}$ is shown for each system in Table I. In addition, Table I lists the states that are treated as core electrons, the used lattice constant $a_0$, the employed muffin-tin radii, the plane-wave cutoff $G_{max}$ of the LAPW basis, and the plane-wave cutoff $G_{max}^{dop}$ used for expanding the density and potential. A rather high value of $G_{max}^{dop}$ is necessary for the LEVEL 3 surface force term containing the xc energy density, since the latter contains fractional powers of the density and thus requires a large cutoff in Fourier space to sample them properly [31].

### A. Analytic vs numerical force

Instead of applying the force formula, Eq. (12), the atomic force on atom $\alpha$ can be computed from the numerical derivative of the total energy with respect to the displacement of atom $\alpha$. We compare the numerical force with that obtained from the force formula for the case of rocksalt MgO and for the different LEVELs of the force implementation.

Figure 2(a) shows the force on the Mg atom resulting from the displacement $\Delta\tau$ of the Mg atom from its equilibrium position along the [100] direction. The resulting force points in the opposite direction and is shown on the ordinate in Fig. 2(a). Each symbol corresponds to a self-consistent calculation for which the total energy and the forces have been evaluated. The (black) dots are the force according to Eq. (12) at LEVEL 0, where the (red) diamonds correspond to the force at LEVEL 3. The dashed (black) line corresponds to the force obtained from the numerical differentiation of the quadratic fit to the energy versus displacement data points shown in the inset

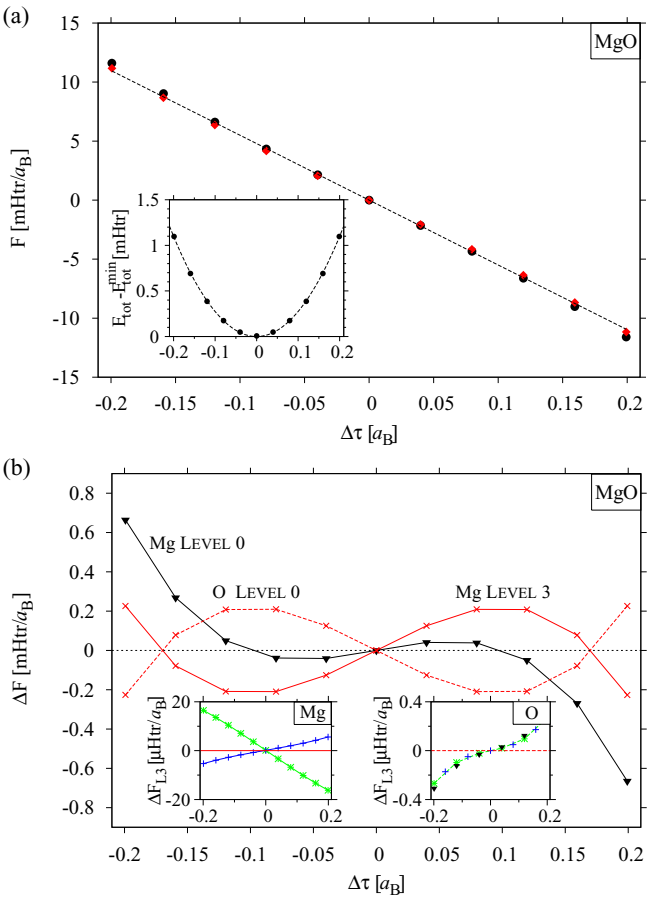


FIG. 2. (Color online) (a) Comparison of the numerical differentiated force [(black) dashed line] with the force at LEVEL 0 [(black) dots] and LEVEL 3 [(red) diamonds]. The inset shows the energy versus displacement curve from which the numerical differentiated force results. (b) The deviation $\Delta F$ of the force at LEVEL 0 [(black) triangles] and LEVEL 3 [(red) crosses] from the numerical differentiated one is shown for the Mg (full lines) and O (dashed lines) atoms. The differences between the force at the different LEVELs with respect to LEVEL 3 is shown in the inset [LEVEL 0: (black) triangles; LEVEL 1: (green) asterisks; LEVEL 2: (blue) pluses; LEVEL 3: (red) zero line]. Please note the different scale.

of the figure. The force at LEVEL 0 and LEVEL 3 agrees quite well with the numerically differentiated force. While for small displacements the force at LEVEL 0 is in slightly better agreement with the numerical derivative, it is the other way around for larger displacements. (The forces at LEVEL 1 and LEVEL 2, respectively, are not shown, since on the scale of the graph the differences between LEVELs 1, 2, and 3 are hardly visible.)

In order to analyze the difference between numerical and analytic force in more detail, we show in Fig. 2(b) the difference $\Delta F$ between the numerical force and the force at LEVEL 0 and LEVEL 3. The aforementioned trend becomes clearly visible, now. However, the force on the Mg atom at LEVEL 0 is not consistent with the force acting on the oxygen atom [dashed (red) line], which is (nearly) the same at all LEVELs [see inset of Fig. 2(b)]. According to Newton's third law one expects that the force on the O atom is the negative of

the force on the Mg atom. It becomes evident from Fig. 2(b), that this is not the case at LEVEL 0. At least LEVEL 1 is required to recover this symmetry. The differences between the force at LEVEL 1 and LEVEL 2 with respect to LEVEL 3 are shown in the inset of Fig. 2(b) for the Mg and O atoms. For the O atom, also the difference between LEVEL 0 and LEVEL 3 is depicted within the same inset.

In conclusion, at least LEVEL 1, i.e., the inclusion of the whole unit cell into the calculation of the Pulay core forces, Eq. (20), is necessary to give rise to a force on the Mg atom, which is consistent with the force on the O atom. The better agreement of the force acting on Mg at LEVEL 0 with the numerical differentiated value for small displacements seems to be fortuitous.

### B. Drift force

The translational invariance of the total energy with respect to the displacement of all atoms by a translational vector $\mathbf{T}$, i.e., $E[\{\boldsymbol{\tau}_\alpha\}] = E[\{\boldsymbol{\tau}_\alpha + \mathbf{T}\}]$, entails that the force summed over all atoms of the unit cell has to vanish—the so-called acoustic sum rule. A spuriously remaining force corresponds to an unphysical energy gain by an arbitrary shift of the whole system. In practice we found a spuriously remaining force and refer to this force as the drift force.

We demonstrate in Tables II and III that the force computed at LEVEL 0 in general violates this sum rule. The largest drift is observed for MgO with the Mg $2s$ and $2p$ electrons treated as core states. The remaining force amounts to $-0.44$ mHtr/$a_B$. The main source for violating the translational invariance originates from the improper inclusion of the tails of the core electrons. This is substantiated by the calculations at LEVEL 1, at which the absolute drift is reduced to less than 0.02 mHtr/$a_B$ for MgO and 0.06 mHtr/$a_B$ for $EuTiO_3$. Moreover, the MgO calculation with the Mg $2s$ and $2p$ as valence electrons supports this thesis [cf. Table II(b)] [32]. Further improvement can be achieved by the proper evaluation of the kinetic energy surface term (LEVEL 2) and the additional surface terms (LEVEL 3).

The convergence of the drift term with respect to $l_{max}$ is analyzed in the following. Figures 3 and 4 show for MgO and $EuTiO_3$, respectively, that at LEVEL 0 the drift term exhibits a slow convergence to a constant nonzero value. At LEVEL 1 this offset is removed, which exemplifies again the systematic error done by ignoring the tails of the core electrons leaking out of the MT sphere. Though the curve still exhibits a rather slow convergence with respect to $l_{max}$. Taking into account the discontinuities at the MT sphere boundaries for the kinetic energy (LEVEL 2) and charge density and potential (LEVEL 3) accelerates the convergence in terms of the angular momentum cutoff. In particular, in the low-$l_{max}$ cases the change in the drift force due to LEVEL 2 is of the same order of magnitude as the shift by employing LEVEL 1 and it is mandatory for the further improvement by using LEVEL 3, which typically yields the best

TABLE II. Force (in mHtr/$a_B$) on the Mg and O atoms of MgO for the different implementation LEVELs and for a calculation with the Mg $2s$ and $2p$ states as core electrons in (a) and as valence electrons in (b). For both calculations the Mg sublattice has been displaced by $0.199a_B$ along the [100] direction with respect to the O sublattice.

(a)

| Force on | LEVEL 0 | LEVEL 1 | LEVEL 2 | LEVEL 3 |
|---|---|---|---|---|
| Mg | −11.6046 | −11.1820 | −11.1603 | −11.1655 |
| O | 11.1652 | 11.1652 | 11.1652 | 11.1649 |
| Drift | −0.4394 | −0.0168 | 0.0049 | −0.0006 |

(b)

| Force on | LEVEL 0 | LEVEL 1 | LEVEL 2 | LEVEL 3 |
|---|---|---|---|---|
| Mg | −10.8027 | −10.8027 | −10.7809 | −10.7861 |
| O | 10.7857 | 10.7857 | 10.7857 | 10.7854 |
| Drift | −0.0170 | −0.0170 | 0.0048 | −0.0007 |

TABLE III. Same as Table II for $EuTiO_3$, but the titanium atom Ti has been displaced by $0.022a_B$ in the [100] direction. The angular momentum cutoff $l_{max}$ is set to 10 in (a) and 12 in (b).

(a)

| Force on | LEVEL 0 | LEVEL 1 | LEVEL 2 | LEVEL 3 |
|---|---|---|---|---|
| Eu | 0.6215 | 0.6215 | 0.6213 | 0.6214 |
| $O_{0\frac{1}{2}\frac{1}{2}}$ | 0.8866 | 0.8866 | 0.8866 | 0.8865 |
| $O_{\frac{1}{2}0\frac{1}{2}/\frac{1}{2}\frac{1}{2}0}$ | 0.2335 | 0.2335 | 0.2335 | 0.2335 |
| Ti | −2.1101 | −2.0283 | −1.9520 | −1.9705 |
| Drift | 0.1350 | −0.0532 | 0.0229 | 0.0044 |

(b)

| Force on | LEVEL 0 | LEVEL 1 | LEVEL 2 | LEVEL 3 |
|---|---|---|---|---|
| Eu | 0.6213 | 0.6213 | 0.6213 | 0.6213 |
| $O_{0\frac{1}{2}\frac{1}{2}}$ | 0.8798 | 0.8798 | 0.8798 | 0.8797 |
| $O_{\frac{1}{2}0\frac{1}{2}/\frac{1}{2}\frac{1}{2}0}$ | 0.2330 | 0.2330 | 0.2330 | 0.2330 |
| Ti | −2.0501 | −1.9686 | −1.9664 | −1.9680 |
| Drift | −0.0830 | −0.0015 | 0.0007 | −0.0010 |

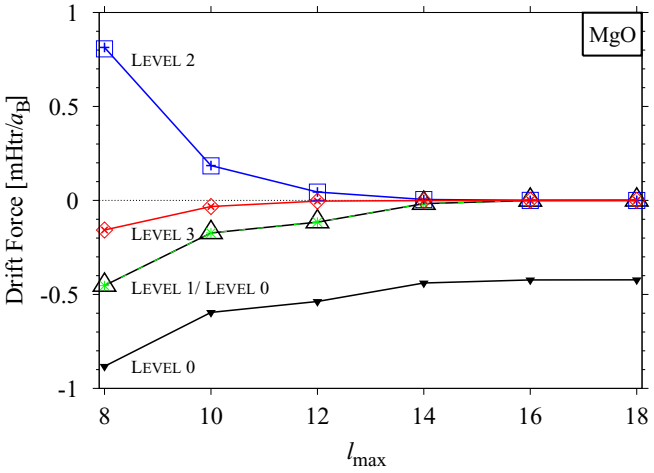


FIG. 3. (Color online) Drift force of MgO (for the same displacement as applied in Table II) as a function of the angular momentum cutoff value $l_{max}$ and for the different force LEVELs. Small (black) triangles, (green) asterisks, (blue) pluses, and (red) crosses correspond to LEVELs 0, 1, 2, and 3 for a calculation with the Mg $2s$ and $2p$ states as core electrons. Large (black) open triangles, (blue) open squares, and (red) open diamonds correspond to LEVELs 0, 2, and 3 of a calculation where the Mg $2s$ and $2p$ states are treated as valence electrons. LEVEL 1 gives the same drift force as LEVEL 0 in this case.

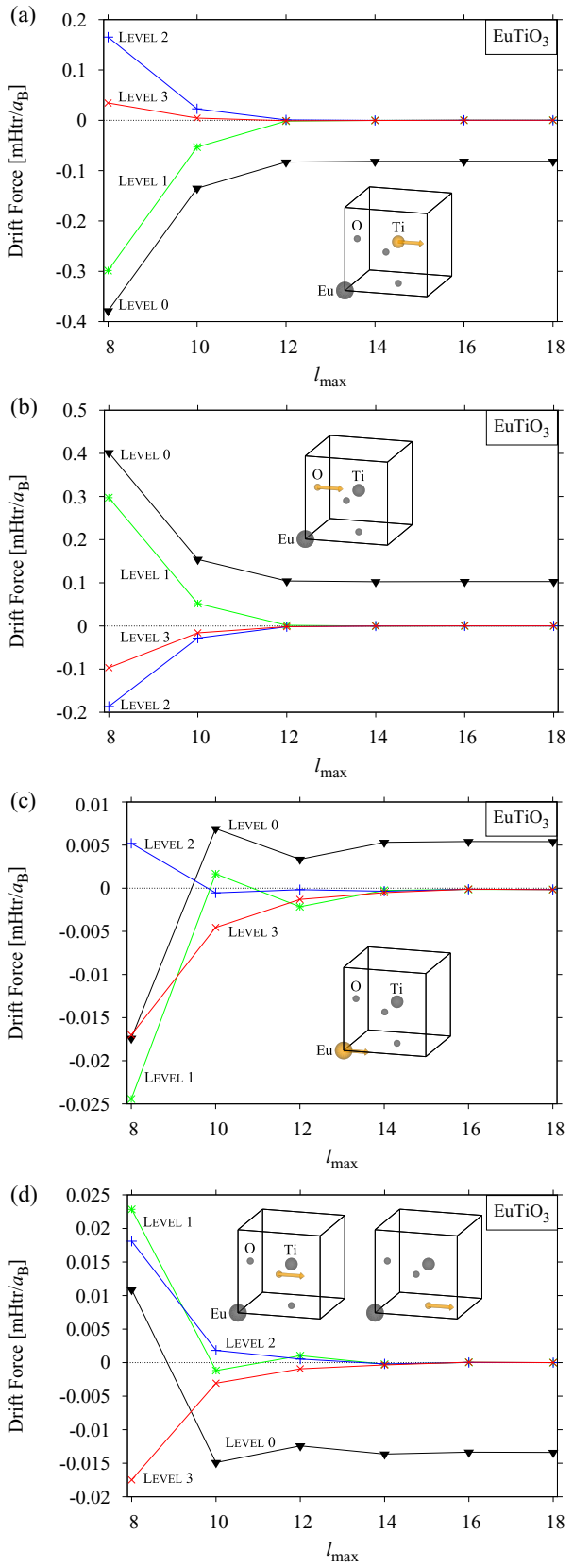


FIG. 4. (Color online) Drift force of $EuTiO_3$ with respect to the angular momentum cutoff $l_{max}$ and the different force LEVELs [LEVEL 0: (black) triangles; LEVEL 1: (green) asterisks; LEVEL 2: (blue) pluses; LEVEL 3: (red) crosses]. In each subfigure a different atom is displaced by $0.022a_B$ along the [100] direction as indicated in the inset.

convergence in terms of $l_{max}$. However, if the spurious drift force is in the range of a few $\mu$Htr/$a_B$ already at LEVEL 0 or if the calculation is already converged to that accuracy, a clear hierarchy between LEVELs 1, 2, and 3 cannot be identified [see Figs. 4(c), 4(d), and Table III(b)]. This means that $\mu$Htr/$a_B$ is the limit in accuracy of our current implementation. For MgO it is noteworthy that at the first, second, and third LEVELs the convergence is independent of the treatment of the Mg $2s$ and $2p$ core states. For all three LEVELs the convergence curves lie on top of each other (see Fig. 3), irrespective of the treatment of the core electrons.

In conclusion, with the force formula at LEVEL 3 the acoustic sum rule can be fulfilled with an accuracy of about $2\mu$Htr/$a_B$ at a rather modest angular momentum cutoff of about 12.

### C. Force constant matrix

The acoustic sum rule is intimately connected with and in fact guarantees the Goldstone mode of the acoustic phonons, i.e., that the three acoustic phonon branches have zero energy at the $\Gamma$ point of the BZ. In the perspective of phonon calculations based on the finite displacement method the improved realization of the acoustic sum rule thus directly transfers to an enhanced fulfillment of the Goldstone mode of the acoustic phonon branches.

The central quantity for phonon calculations based on the finite displacement approach is the force matrix $F_{\gamma lj,\beta ki}$, which is composed of the force acting on atom $\gamma$ of unit cell $l$ along direction $j$ caused by displacing atom $\beta$ of unit cell $k$ along direction $i$. This displacement is denoted as $u_{\beta ki}$. From the force matrix, the force-constant matrix $\Phi_{\beta ki,\gamma lj}$, which is defined as the second derivative of the total energy with respect to the atomic displacements

$$\Phi_{\beta ki,\gamma lj} = \frac{\partial^2 E}{\partial \tau_{\beta ki} \partial \tau_{\gamma li}}, \tag{23}$$

can be approximated by

$$\Phi_{\beta ki,\gamma lj} \approx -\frac{F_{\gamma lj,\beta ki}}{u_{\beta ki}}. \tag{24}$$

By Young's theorem, the force-constant matrix has to be symmetric ($\Phi_{\beta ki,\gamma lj} = \Phi_{\gamma lj,\beta ki}$). If the displacements $u_{\beta ki}$ are of the same length, the force matrix has to exhibit the same symmetry. The dynamical matrix is related to the force-constant matrix by a Fourier transform and its eigenvalues are proportional to the squares of the phonon frequencies.

For $EuTiO_3$ we have displaced each atom of the unit cell by the same length and analyzed the symmetry of the force matrix. In fact, we restrict ourselves to displacements along the [100] direction and show the corresponding forces along the same direction. In Table IV the respective part of the force matrix is shown for LEVEL 0 and LEVEL 3 of the force implementation. At the former LEVEL we observe maximal absolute deviations from symmetry of 103.2 $\mu$Htr/$a_B$ and an averaged deviation of about 14.39 $\mu$Htr/$a_B$. The maximal break of symmetry corresponds to a movement of the titanium atom towards an oxygen atom, or vice versa. By comparison of the two force matrices it becomes evident that, in particular, the force on the Ti atom resulting from the movement of the different atoms is

TABLE IV. Part of the force matrix of $EuTiO_3$ in $\mu\mathrm{Htr}/a_\mathrm{B}$ for force LEVEL 0 in (a) and for LEVEL 3 in (b). The first column of a row lists the atom which has been displaced by $0.022a_\mathrm{B}$ along the [100] direction. The component of the force along the same direction is then shown for each atom in the unit cell. In the last column (row) the force values of each row (column) are summed up.

(a) LEVEL 0

| | Eu | $O_{0\frac{1}{2}\frac{1}{2}}$ | $O_{\frac{1}{2}0\frac{1}{2}}$ | $O_{\frac{1}{2}\frac{1}{2}0}$ | Ti | Drift |
|---|---|---|---|---|---|---|
| $Eu_{000}$ | −274.4 | 200.3 | −274.6 | −274.6 | 626.7 | 3.4 |
| $O_{0\frac{1}{2}\frac{1}{2}}$ | 199.0 | −3208.7 | 1065.5 | 1065.5 | 983.0 | 104.3 |
| $O_{\frac{1}{2}0\frac{1}{2}}$ | −273.0 | 1067.0 | −832.5 | −193.4 | 219.5 | −12.4 |
| $O_{\frac{1}{2}\frac{1}{2}0}$ | −273.0 | 1067.0 | −194.2 | −831.8 | 219.6 | −12.4 |
| $Ti_{\frac{1}{2}\frac{1}{2}\frac{1}{2}}$ | 621.3 | 879.8 | 233.0 | 233.0 | −2050.1 | −83.0 |
| Total | −0.1 | 5.4 | −2.8 | −1.3 | −1.3 | – |

Maximal/average deviation from symmetry: 103.2/14.39

(b) LEVEL 3

| | Eu | $O_{0\frac{1}{2}\frac{1}{2}}$ | $O_{\frac{1}{2}0\frac{1}{2}}$ | $O_{\frac{1}{2}\frac{1}{2}0}$ | Ti | Drift |
|---|---|---|---|---|---|---|
| $Eu_{000}$ | −272.2 | 200.3 | −274.6 | −274.6 | 619.9 | −1.2 |
| $O_{0\frac{1}{2}\frac{1}{2}}$ | 199.2 | −3208.7 | 1065.5 | 1065.5 | 876.9 | −1.6 |
| $O_{\frac{1}{2}0\frac{1}{2}}$ | −274.3 | 1067.0 | −832.5 | −193.4 | 232.2 | −1.0 |
| $O_{\frac{1}{2}\frac{1}{2}0}$ | −274.3 | 1067.0 | −194.2 | −831.7 | 232.3 | −0.9 |
| $Ti_{\frac{1}{2}\frac{1}{2}\frac{1}{2}}$ | 621.3 | 879.7 | 233.0 | 233.0 | −1968.0 | −1.0 |
| Total | −0.3 | 5.3 | −2.8 | −1.2 | −6.7 | – |

Maximal/average deviation from symmetry: 2.8/1.15

affected. This is reasonable as among the different atoms of $EuTiO_3$ the core electrons of the Ti atom exhibit the largest charge density outside of their MT sphere, which is completely ignored at LEVEL 0. With the refined force at LEVEL 3 the maximal deviation from a symmetric form reduces by two orders of magnitude to 2.8 $\mu\mathrm{Htr}/a_\mathrm{B}$ and is still given by the displacement of the titanium atoms towards the oxygen ones. Likewise the averaged deviation reduces to 1.15 $\mu\mathrm{Htr}/a_\mathrm{B}$. Interestingly, the sum of the forces acting on one atom, i.e., the sum of the forces in each column, adds up to about 1 $\mu\mathrm{Htr}/a_\mathrm{B}$ already at LEVEL 0. As we add up forces coming from different and independent calculations in this case, these values can be regarded to define an ultimate accuracy limit for the force matrix. The rows of the force matrix, stemming from one calculation, exhibit a sizable larger error at LEVEL 0. At LEVEL 3 we achieve an accuracy in the rows and columns of equal quality. [It is this limit in accuracy that is already achieved in Table III(b) at LEVEL 1.]

### D. Computational workload

To complete the discussion of LEVELS 1, 2, and 3, we address the computational overhead caused by each of these LEVELS in this section.

As the forces are typically calculated after a self-consistent charge density is found, we quantify the computational overhead for each LEVEL with respect to the average time required for a single iteration of the self-consistent-field (SCF) cycle and list the additional computation time of each LEVEL with respect to the average SCF time in Table V.

For MgO the computation of the atomic force at LEVEL 0 leads to an increase of the computation time by 15%.

TABLE V. Computational overhead for computing the atomic force at the different force LEVELS (a) for MgO and (b) for $EuTiO_3$. The percentage values are given with respect to the average time of a single iteration of the SCF cycle (MgO: 124.3 s for $Mg_{core}$:[He]$2s2p$ and 129.2 s for $Mg_{core}$:[He]; $EuTiO_3$: 825.7 s for $G_\mathrm{max}^\mathrm{dop} = 28.81a_\mathrm{B}^{-1}$ and 746.0 s for $G_\mathrm{max}^\mathrm{dop} = 19.21a_\mathrm{B}^{-1}$ calculated on a single Intel Xeon CPU X5670 @ 2.93 GHz). In the case of MgO also the relative increase in total computation time is shown when the Mg $2s2p$ are treated as valence electrons by adding local orbitals. For $EuTiO_3$ timings for two different $G_\mathrm{max}^\mathrm{dop}$ cutoffs are shown.

(a)

| MgO | LEVEL 0 | LEVEL 1 | LEVEL 2 | LEVEL 3 |
|---|---|---|---|---|
| $Mg_{core}$: [He]$2s2p$ | +15.2% | +3.4% | −0.9% | +0.3% |
| $Mg_{core}$: [He] | +20.5% | +2.7% | +1.2% | +0.1% |
| Relative increase | 8.8% | 8.1% | 9.8% | 9.7% |

(b)

| $EuTiO_3$ | LEVEL 0 | LEVEL 1 | LEVEL 2 | LEVEL 3 |
|---|---|---|---|---|
| $G_\mathrm{max}^\mathrm{dop} = 28.81a_\mathrm{B}^{-1}$ | +11.2% | +16.7% | +5.8% | +1.4% |
| $G_\mathrm{max}^\mathrm{dop} = 19.21a_\mathrm{B}^{-1}$ | +12.8% | +5.3% | +6.5% | +0.8% |

LEVELS 1, 2, and 3 require only a small additional amount of time. In total, LEVEL 3 gives rise to an overhead of less than 3%. The negative percentage value at LEVEL 2 corresponds to a gain in speed and can be understood by the fact that at LEVEL 2 we replace the original evaluation of the kinetic surface term by our formulation instead of adding it on top. For the special case of MgO, this replacement in fact requires less time than the original implementation. In addition, we show timings for MgO, where the Mg $2s$ and $2p$ states are treated as valence states by local orbitals. In comparison to the calculation without local orbitals the time per SCF cycle increases by 4% and the total computation time for each force LEVEL grows by about 9%.

The timings of $EuTiO_3$ belong to a displacement of the $O_{\frac{1}{2}0\frac{1}{2}}$ atom within the europium plane by $0.022a_\mathrm{B}$ along the [100] direction. All other possible displacements for $EuTiO_3$ lead to a crystal structure which exhibits at least the same or a higher spatial symmetry. Hence, the computing time benefits least from the available symmetry operations. The largest overhead is caused by LEVEL 1, which requires even more time than LEVEL 0. On top, LEVELS 2 and 3 lead merely to an increase of about 6% and 1%, respectively. The rather high computational demand of LEVEL 1 is caused by the large reciprocal cutoff value $G_\mathrm{max}^\mathrm{dop}$ for expanding the density or the potential. This large cutoff is required for the surface force term at LEVEL 3, whereas LEVELS 1 and 2 are rather insensitive to this parameter. For example, reducing $G_\mathrm{max}^\mathrm{dop}$ to $19.21a_\mathrm{B}$ decreases the computation time for LEVEL 1 to 5%. Thus, it can be more efficient to omit LEVEL 3 and stick instead to LEVEL 2 with a small $G_\mathrm{max}^\mathrm{dop}$ and an increased $l_\mathrm{max}$ cutoff.

We conclude by noting that among the three LEVELS 1, 2, and 3, eventually the second LEVEL will become the computationally most expensive one in the limit of large systems, since it shows a scaling with the third power of the system size just as LEVEL 0, while LEVELS 1 and 3 scale with the system size squared (see Appendix B).

## V. CONCLUSIONS

In this work, we presented a robust algorithm for calculating the atomic force with an accuracy of $\mu\mathrm{Htr}/a_\mathrm{B}$ within the all-electron FLAPW method employing the conventional LAPW basis set. This was achieved by refining the force formalism of Yu *et al.* [12]: The tails of energetically high-lying core-electron states are taken into account and the slight discontinuities of LAPW basis function, density, and potential at the MT sphere boundaries are explicitly considered giving rise to additional surface force terms. Although the force contribution of these high-lying core states can also be treated through local orbitals, the additional force term (LEVEL 1) accounts only for a fraction of the overall CPU time to calculate the force and is thus a viable alternative in balancing the choice of the muffin-tin sphere radius and computational efficiency. In a worst case scenario of an $f$-electron system at low symmetry the addition of all improvements may increase the CPU time required solely for calculating the force by a factor of 2 up to 3, which is still negligible in comparison to the total CPU time of an electronic structure calculation. The implementations of these corrections are straightforward and can be taken over easily into any realization of the FLAPW method working with the Yu *et al.* [12] formulation of the force.

We demonstrated for MgO and $EuTiO_3$ that the inclusion of the tail of the core-electron states is crucial to fulfill the acoustic sum rule, which is otherwise violated. The additional surface terms, on the contrary, improve the convergence of the force with respect to the angular momentum cutoff of the LAPW basis functions in the muffin-tin spheres—an inherent numerical parameter of the LAPW approach.

Phonon calculations within the finite displacement method should directly benefit from the presented amendments to the atomic force. Moreover, the same line of arguments that led to the refined atomic force applies to the calculation of force constants in density functional perturbation theory (DFPT) [33,34]. Hence, the amendments to the atomic force might also be important for calculating phonons in DFPT.

## ACKNOWLEDGMENTS

We thank K. Rushchanskii and G. Bihlmayer for enlightening discussions. M.B. gratefully acknowledges financial support from the Helmholtz Association through the Helmholtz Postdoc Programme (VH-PD-022).

## APPENDIX A: CALCULATION OF $\mathbf{F}^{\mathrm{Pulay}}_{\alpha,\mathrm{core}}$

While the contribution of the MT sphere of the moving atom $\alpha$ to the core Pulay term [Eq. (20)] can be computed straightforwardly, we explain the contributions of the IR and the other MT spheres ($\beta \neq \alpha$) in more detail in the following. As discussed in Sec. II the tail of the core charge density is expanded in plane waves. Thus, the gradient of the core tail charge density is given by

$$\begin{aligned}\nabla\rho^{\alpha}_{\mathrm{core}}(\mathbf{r}) &= \sum_{\mathbf{G}} i\mathbf{G}\rho^{\alpha}_{\mathrm{core}}(\mathbf{G})\exp(i\mathbf{G}\cdot\mathbf{r})\\ &=: \sum_{\mathbf{G}}\left[\nabla\boldsymbol{\rho}^{\boldsymbol{\alpha}}_{\mathbf{core}}\right](\mathbf{G})\exp(i\mathbf{G}\cdot\mathbf{r}),\end{aligned} \tag{A1}$$

and the interstitial part of Eq. (20) becomes

$$\begin{aligned}\mathbf{F}^{\mathrm{Pulay,IR}}_{\alpha,\mathrm{core}} &= \int_{\mathrm{IR}} V_{\mathrm{eff}}(\mathbf{r})\nabla\rho^{\alpha}_{\mathrm{core}}(\mathbf{r})d^3r\\ &= \int_{\Omega}\left(\Theta_{\mathrm{IR}}V_{\mathrm{eff}}\right)(\mathbf{r})\nabla\rho^{\alpha}_{\mathrm{core}}(\mathbf{r})d^3r\\ &= \Omega\sum_{\mathbf{G}}(\Theta_{\mathrm{IR}}V_{\mathrm{eff}})^{*}(\mathbf{G})\left[\nabla\boldsymbol{\rho}^{\boldsymbol{\alpha}}_{\mathbf{core}}\right](\mathbf{G}),\end{aligned} \tag{A2}$$

where the integral over the IR has been expanded over the whole unit cell by introducing the Heaviside step function $\Theta_{\mathrm{IR}}(\mathbf{r})$, which is 1 in the interstitial region and 0 in the muffin-tin spheres. The contribution from the MT spheres with $\beta \neq \alpha$ remains and reads

$$\begin{aligned}\mathbf{F}^{\mathrm{Pulay,MTs}}_{\alpha,\mathrm{core}} &= \sum_{\beta\neq\alpha}\int_{\mathrm{MT}(\beta)} V_{\mathrm{eff}}(\mathbf{r})\nabla\rho^{\alpha}_{\mathrm{core}}(\mathbf{r})d^3r\\ &= \sum_{\beta}\int_{\mathrm{MT}(\beta)} V_{\mathrm{eff}}(\mathbf{r})\nabla\rho^{\alpha}_{\mathrm{core}}(\mathbf{r})d^3r\\ &\quad - \int_{\mathrm{MT}(\alpha)} V_{\mathrm{eff}}(\mathbf{r})\nabla\rho^{\alpha}_{\mathrm{core}}(\mathbf{r})d^3r.\end{aligned} \tag{A3}$$

Computationally it is favorable to run over all MT spheres and subtract the contribution from the MT sphere $\alpha$ afterwards, since then a part of the integral becomes independent from the atom $\alpha$ and can be precalculated for each $\mathbf{G}$:

$$\begin{aligned}&\sum_{\beta}\int_{\mathrm{MT}(\beta)} V_{\mathrm{eff}}(\mathbf{r})\nabla\rho^{\alpha}_{\mathrm{core}}(\mathbf{r})d^3r\\ &= \sum_{\mathbf{G}}\left[\nabla\boldsymbol{\rho}^{\boldsymbol{\alpha}}_{\mathbf{core}}\right](\mathbf{G})\sum_{\beta}e^{i\mathbf{G}\cdot\boldsymbol{\tau}_\beta}\\ &\quad\times\int_0^{R_\beta} r^2\sum_{lm}4\pi i^l Y^{*}_{lm}(\hat{\mathbf{G}})j_l(Gr)V^{\beta *}_{\mathrm{eff}lm}(r)dr.\end{aligned} \tag{A4}$$

Finally, we have to subtract

$$\begin{aligned}&\int_{\mathrm{MT}(\alpha)} V_{\mathrm{eff}}(\mathbf{r})\nabla\rho^{\alpha}_{\mathrm{core}}(\mathbf{r})d^3r\\ &= \sum_{\mathbf{G}}\left[\nabla\boldsymbol{\rho}^{\boldsymbol{\alpha}}_{\mathbf{core}}\right](\mathbf{G})e^{i\mathbf{G}\cdot\boldsymbol{\tau}_\alpha}\\ &\quad\times\int_0^{R_\alpha} r^2\sum_{lm}4\pi i^l Y^{*}_{lm}(\hat{\mathbf{G}})j_l(Gr)V^{\alpha *}_{\mathrm{eff}lm}(r)dr.\end{aligned} \tag{A5}$$

We note that in this way a quadratic scaling of the core Pulay term with the system size is achieved.

## APPENDIX B: IR SURFACE TERMS

In order to evaluate the surface integrals of the kind

$$\oint_{\partial\mathrm{MT}(\alpha)} f^{\mathrm{IR}}(\mathbf{r})g^{\mathrm{IR}}(\mathbf{r})\hat{\mathbf{e}}\,dS, \tag{B1}$$

where $f^{\mathrm{IR}}(\mathbf{r})$, $g^{\mathrm{IR}}(\mathbf{r})$ stand for the IR representation of wave function, density, or potential, we expand $f^{\mathrm{IR}}(\mathbf{r})$, $g^{\mathrm{IR}}(\mathbf{r})$ into spherical harmonics centered at atomic position $\boldsymbol{\tau}_\alpha$ by using the Rayleigh expansion, e.g.,

$$\begin{aligned} f^{\mathrm{IR}}(\mathbf{r}) &= \sum_{\mathbf{G}}^{G<G_{\max}} f(\mathbf{G}) \exp(i\mathbf{G}\cdot\mathbf{r}) \\ &= \sum_{lm}\left[4\pi i^l \sum_{\mathbf{G}}^{G<G_{\max}} f(\mathbf{G}) Y^*_{lm}(\hat{\mathbf{G}}) j_l(Gr) e^{i\mathbf{G}\cdot\boldsymbol{\tau}_\alpha}\right] Y_{lm}(\hat{\mathbf{r}}_\alpha) \\ &=: \sum_{lm} f^\alpha_{lm}(r_\alpha) Y_{lm}(\hat{\mathbf{r}}_\alpha), \end{aligned} \tag{B2}$$

where we switched to the local coordinate frame $\mathbf{r}_\alpha = \mathbf{r} - \boldsymbol{\tau}_\alpha$. Likewise, the unit vector $\hat{\mathbf{e}}$, which corresponds to $\hat{\mathbf{r}}_\alpha$, is expressed in spherical harmonics within the Cartesian basis $\hat{\mathbf{e}}_i$ as

$$\begin{aligned} \hat{\mathbf{e}} &= \sum_{i=1}^{3}\sum_{m=-1}^{1} c_{i,m} Y_{1m}(\hat{\mathbf{e}})\hat{\mathbf{e}}_i \\ &:= \sqrt{2\pi/3}\begin{pmatrix} Y_{1-1}(\hat{\mathbf{e}}) - Y_{11}(\hat{\mathbf{e}}) \\ iY_{1-1}(\hat{\mathbf{e}}) + iY_{11}(\hat{\mathbf{e}}) \\ \sqrt{2}Y_{10}(\hat{\mathbf{e}}) \end{pmatrix}. \end{aligned} \tag{B3}$$

In practice, we truncated the $lm$ expansion in Eq. (B2) at $l = 2l_{\max}$ and thus we obtain for the surface integral

$$\begin{aligned} &\oint_{\partial \mathrm{MT}(\alpha)} f^{\mathrm{IR}}(\mathbf{r}) g^{\mathrm{IR}}(\mathbf{r}) \hat{\mathbf{e}}\, dS \\ &= R_\alpha^2 \sum_i \hat{\mathbf{e}}_i \sum_{l=0}^{2l_{\max}} \sum_{l'=|l-1|}^{\min(l+1,2l_{\max}),2} \\ &\quad\times \sum_{m=-l}^{l}\sum_{m''=-1}^{1} c^*_{i,m''} f^\alpha_{lm}(R_\alpha) g^\alpha_{l'm'}(R_\alpha) G^{m'',m,m'}_{1,l,l'} \end{aligned} \tag{B4}$$

with the Gaunt coefficient $G^{m'',m,m'}_{1,l,l'} = \oint Y^*_{1m''}(\hat{\mathbf{r}}) Y_{lm}(\hat{\mathbf{r}}) Y_{l'm'}(\hat{\mathbf{r}}) d\hat{S}$. The latter is only nonzero for $|l-1| \leqslant l' \leqslant l+1$ with $l + l' + 1$ even and $m' = m'' - m$, to which $m'$ is set in the expression above.

The IR surface terms of Eq. (14) comprising the interstitial density, interstitial potential, or interstitial xc energy density are computed by employing Eq. (B4). These surface integrals exhibit a scaling with the square of the system size.

The kinetic energy surface term of Eq. (22) can be computed for each occupied wave function as explained above if one identifies $\varphi^{\mathrm{IR}*}_{n\mathbf{k}}(\mathbf{r})$ with $f^{\mathrm{IR}}(\mathbf{r})$ and $[T - \epsilon_{n\mathbf{k}}]\varphi^{\mathrm{IR}}_{n\mathbf{k}}(\mathbf{r})$ with $g^{\mathrm{IR}}(\mathbf{r})$. The additional summation over the occupied states increases the complexity for the kinetic energy surface term to cubic.


[1] P. Hohenberg and W. Kohn, Phys. Rev. **136**, B864 (1964).
[2] *A Primer in Density Functional Theory*, edited by C. Fiolhais, F. Nogueira, and M. A. L. Marques, Lecture Notes in Physics (Springer, Heidelberg, 2003), Vol. 620.
[3] W. Kohn and L. J. Sham, Phys. Rev. **140**, A1133 (1965).
[4] R. Fletcher, *Practical Methods of Optimization* (Wiley, Chichester, 1980).
[5] G. Kresse, J. Furthmüller, and J. Hafner, Europhys. Lett. **32**, 729 (1995).
[6] D. Alfè, G. D. Price, and M. J. Gillan, Phys. Rev. B **64**, 045123 (2001).
[7] A. Togo, F. Oba, and I. Tanaka, Phys. Rev. B **78**, 134106 (2008).
[8] The number of necessary displacements can be reduced by exploiting spatial symmetry.
[9] E. Wimmer, H. Krakauer, M. Weinert, and A. J. Freeman, Phys. Rev. B **24**, 864 (1981).
[10] M. Weinert, E. Wimmer, and A. J. Freeman, Phys. Rev. B **26**, 4571 (1982).
[11] H. J. F. Jansen and A. J. Freeman, Phys. Rev. B **30**, 561 (1984).
[12] R. Yu, D. Singh, and H. Krakauer, Phys. Rev. B **43**, 6411 (1991).
[13] J. M. Soler and A. R. Williams, Phys. Rev. B **40**, 1560 (1989).
[14] J. M. Soler and A. R. Williams, Phys. Rev. B **42**, 9728 (1990).
[15] P. Pulay, Mol. Phys. **17**, 197 (1969).
[16] J. M. Soler and A. R. Williams, Phys. Rev. B **47**, 6784 (1993).
[17] M. Fähnle, C. Elsässer, and H. G. Krimmel, Phys. Status Solidi B **191**, 9 (1995).
[18] D. M. Ceperley and B. J. Alder, Phys. Rev. Lett. **45**, 566 (1980).
[19] S. H. Vosko, L. Wilk, and M. Nusair, Can. J. Phys. **58**, 1200 (1980).
[20] G. Michalicek, M. Betzinger, C. Friedrich, and S. Blügel, Comput. Phys. Commun. **184**, 2670 (2013).
[21] D. Singh, Phys. Rev. B **43**, 6388 (1991).
[22] E. E. Krasovskii, A. N. Yaresko, and V. N. Antonov, J. Electron Spectrosc. Relat. Phenom. **68**, 157 (1994).
[23] C. Friedrich, A. Schindlmayr, S. Blügel, and T. Kotani, Phys. Rev. B **74**, 045104 (2006).
[24] E. E. Krasovskii, Phys. Rev. B **56**, 12866 (1997).
[25] D. J. Singh and L. Nordstrom, *Planewaves, Pseudopotentials and the LAPW Method* (Springer Verlag, Berlin, 2006).
[26] O. K. Andersen, Phys. Rev. B **12**, 3060 (1975).
[27] H. L. Skriver, *The LMTO Method* (Springer, New York, 1984).
[28] M. Methfessel, M. van Schilfgaarde, and R. Casali, in *Electronic Structure and Physical Properies of Solids*, edited by H. Dreysse, Lecture Notes in Physics (Springer, Berlin/Heidelberg, 2000), Vol. 535, pp. 114–147.
[29] M. Weinert and J. W. Davenport, Phys. Rev. B **45**, 13709 (1992).
[30] For the Hellmann-Feynman force term the formalism described in the Appendix of the paper by Yu *et al.* [12] is employed.
[31] Since the volume of integration in LEVEL 3 is restricted to the MT sphere boundary, no orthogonality relations in Fourier space can be used to confine the Fourier expansion to the $G^{\mathrm{dop}}_{\max}$ sufficient for the density.
[32] We attribute the differences in the absolute force values for the two MgO calculations to the different treatment of the Mg $2s$ and $2p$ states. If the latter are considered as core electrons, they only experience the spherical effective potential. On the other hand, if they are treated as valence electrons by adding local orbitals to the LAPW basis set, they perceive the full effective potential.
[33] S. Baroni, S. de Gironcoli, A. Dal Corso, and P. Giannozzi, Rev. Mod. Phys. **73**, 515 (2001).
[34] R. Kouba, A. Taga, C. Ambrosch-Draxl, L. Nordström, and B. Johansson, Phys. Rev. B **64**, 184306 (2001).